Front. Earth Sci. 2012, 6(3): 227–236
DOI 10.1007/s11707-012-0321-3

RESEARCH ARTICLE

Assessing phenological change in China from 1982 to 2006 using AVHRR imagery

Haiyan WEI (✉)[1], Philip HEILMAN[1], Jiaguo QI[2], Mark A. NEARING[1], Zhihui GU[3], Yongguang ZHANG[4]

1 USDA-ARS Southwest Watershed Research Center, AZ 85719, USA
2 Michigan State University, MI 48824-1117, USA
3 Shenzhen University, Shenzhen 518060, China
4 Beijing Normal University, Beijing 100875, China

© Higher Education Press and Springer-Verlag Berlin Heidelberg 2012

Abstract Long-term trends in vegetation phenology indicate ecosystem change due to the combined impacts of human activities and climate. In this study we used 1982 to 2006 Advanced Very High Resolution Radiometer Normalized Difference Vegetation Index (AVHRR NDVI) imagery across China and the TIMESAT program to quantify annual vegetation production and its changing trend. Results showed great spatial variability in vegetation growth and its temporal trend across the country during the 25-year study period. Significant decreases in vegetation production were detected in the grasslands of Inner Mongolia, and in industrializing regions in southern China, including the Pearl River Delta, the Yangtze River Delta, and areas along the Yangtze River. Significant increases in vegetation production were found in Xinjiang, Central China, and North-east China. Validation of the NDVI trends and vegetated area changes were conducted using Landsat imagery and the results were consistent with the analysis from AVHRR data. We also found that although the causes of the vegetation change vary locally, the spatial pattern of the vegetation change and the areas of greatest impact from national policies launched in the 1970s, such as the opening of economic zones and the 'Three-North Shelter Forest Programme', are similar, which indicates an impact of national policies on ecosystem change and that such impacts can be detected using the method described in this paper.

Keywords AVHRR, China, remote sensing, climate change, policy, desertification, temporal trend, phenology

Received November 22, 2011; accepted May 2, 2012

E-mail: haiyan.wei@gmail.com

1 Introduction

Vegetation phenology parameters are indicators of seasonal biologic life stages and have been applied to evaluate climate change impacts on vegetation growth, simulate atmospheric general circulations and carbon sequestration, monitor agricultural production, and detect vegetation growth trends (Piao et al., 2006). Satellite remote sensing provides long-term vegetation index images that can be used to assess long-term phenology changes across large areas (White et al., 1997, 2005; Lucht et al., 2002; Zhang et al., 2003). The Normalized Difference Vegetation Index (NDVI) from the Advanced Very High Resolution Radiometer (AVHRR) of Global Inventory Modeling and Mapping Studies (GIMMS) has the advantage of high temporal resolution since 1980s and is available globally (Tucker et al., 2005). AVHRR NDVI has been used regionally for various purposes, and the quality of AVHRR imagery has proved to be adequate for detecting vegetation change (Eklundh and Jönsson, 2003; Slayback et al., 2003; White et al., 2005; Piao et al., 2006; Raynolds et al., 2006; Zhang et al., 2006).

Extracting phenology change from NDVI typically requires techniques to define the time-span of a growing season and to estimate seasonal production. Methods such as defining NDVI thresholds at the start and end of the growing season and taking the summation or integral of the NDVI curve as an estimate of seasonal production were developed for these purposes (Lloyd, 1990; Markon et al., 1995; Moulin et al., 1997; Raynolds et al., 2006). In this study the TIMESAT program developed by Jönsson and Eklundh (2004) was used because it provides a number of phenological parameters for trend analysis and it has previously been tested using AVHRR data (Jönsson and Eklundh, 2002, 2003, 2004; Lee et al., 2002; Eklundh and Olsson, 2003; Heumann et al., 2007).

Along with the rapid social change and economic growth that have taken place in China in the last several decades as well as climate change, the terrestrial ecosystems and vegetation production have also experienced dramatic changes. Myneni et al. (1997) detected a region between 45°N and 70°N in China with significant increasing trend from 1981 to 1991 using the monthly average 10-day maximum value NDVI composite during the growing season. Piao et al. (2004) found that the mean value of the largest 15-day NDVI composite during the growing season has increased by 81% in their study area (most of China) from 1982 to 1999, and the increase was closely related to an increase in temperature. Similar studies were also conducted in northern China by Tucker et al. (2001) and Zhou et al. (2001). However, the spatial pattern of phenological changes across the country incorporating more recent data remains unknown. The objective of this study is to assess the spatial patterns of vegetation growth trends across China from 1982 to 2006, using AVHRR data.

2 Methodology

Bi-monthly NDVI images derived from the AVHRR sensing system at an 8 km × 8 km spatial resolution during 1982 to 2006 were used in this study. A smoothing algorithm using the adaptive Savitzky-Golay filtering method implemented in TIMESAT was applied to smooth out the noise caused by cloud contamination and atmospheric variability (Chen et al., 2004; Jönsson and Eklundh, 2004). Then a set of phenological parameters including the start and end of growing season, and the estimation of seasonal production were defined and calculated. The start of the growing season was defined as the time when the left edge of NDVI curve in each year increased to 20% of the difference between the peak and base value measured from the left minimum level, and the base values were the average of the minimum values from the left and right edges (Fig. 1); similarly, the end of the growing season was defined as the time when the right edge decreased to 20% of the amplitude measured from the right minimum level; the total seasonal vegetation production was estimated using the integrated area of the region between the NDVI curve and the zero level; the seasonal vegetation growth was calculated as the area between the NDVI curve and the base value during the growing season, which is also called the small integral in TIMESAT, the small integral was used in this paper as it closely approximates annual vegetation production during the growing season.

After the annual small integral value in each year from 1982 to 2006 was calculated for each pixel, an IDL program was written to read these annual integral values, perform a linear regression between the integral values and time (year), save the slope value, and calculate the P value

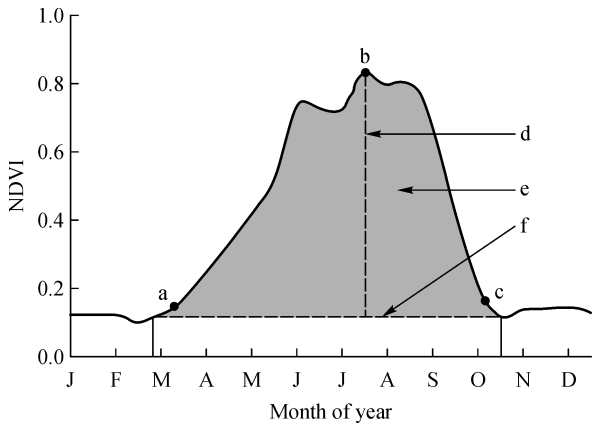

Fig. 1 Seasonal parameters computed in TIMESAT: (a) beginning of season; (b) peak; (c) end of growing season; (d) amplitude; (e) small integral over the growing season, area between NDVI curve and zero level; (f) base value (Adapted from Jönsson and Eklundh, 2004)

of the regression for each pixel. In this study, we considered a relationship with $P \leqslant 0.05$ as a significant trend, and only the slope values with significant trends were used for further analysis.

The pixel size of 8 km × 8 km for AVHRR images allowed us to perform this analysis on a national scale. However, such resolution is relatively coarse, and hence land cover cannot be identified in detail. To validate the results from GIMMS AVHRR data, we also used eight pairs of Landsat images at different locations to compare the NDVI values as well as the vegetation growth trends. The resolutions of the Landsat images ranged from 15 to 60 m. Each pair of Landsat images were taken at a similar time of the year, with one image taken in 1970s or 1980s, and a later one taken in the 2000s. All the Landsat images were first converted from digital numbers to top of atmosphere reflectance (Mather, 2004), then pixel-based NDVI values were calculated using the corresponding bands of each Landsat image as described in the following equation:

$$\mathrm{NDVI} = (\text{Near IR band} - \text{Red band}) / (\text{Near IR band} + \text{Red band}). \quad (1)$$

For each Landsat image the boundary was delineated on the AVHRR image in the corresponding month and year, then on each of the AVHRR images, 10 pixels were randomly selected inside the boundary, and the NDVI values were calculated and compared with the NDVI values averaged from the corresponding Landsat NDVI image.

For the purpose of validation on trend analysis from AVHRR, Landsat images were classified into vegetated and non-vegetated areas. Forest, agriculture, and grassland were classified and grouped into vegetated area. Water, residential use, and bare land were classified as

non-vegetated area. Then changes in the vegetated area were calculated for each location for comparison with the trend analysis results previously obtained from AVHRR images. Land use maps in 1985, 2000, and 2005 were also used to assist classification (Hansen et al., 1998; European Commission, 2003; European Space Agency, 2004–2006).

3 Results

3.1 Trend analysis results

The integrals calculated from TIMESAT vary greatly across China as expected for such a large spatial scale. As an example, Figure 2 shows the spatial distribution of the small integral across China in 1982. The small integral, which is a proxy of the active vegetation production over the growing season, generally increased from the north-west to the south-east of the country. This is a result of the fact that the rainfall increases in this direction, and consequently the vegetation shifts from desert to grass, agriculture and forest, with the annual vegetation production increasing in a similar manner. The small integral is lower in evergreen forests than in the deciduous forests due to the consistently large amount of green vegetation, which results in a high base value for the evergreen forests. As an example, the NDVI time-series for 1982 were plotted in Fig. 3 for a deciduous conifer community extracted in north-eastern China (E'erguna-Zuo Qi, Heilongjiang Province), and an evergreen community from southern China (Sanming City, Guangzhou Province). The comparison showed that the two NDVI time series had similar peak values and lengths of growing season, but different base values and thus different small integral values, or annual growth.

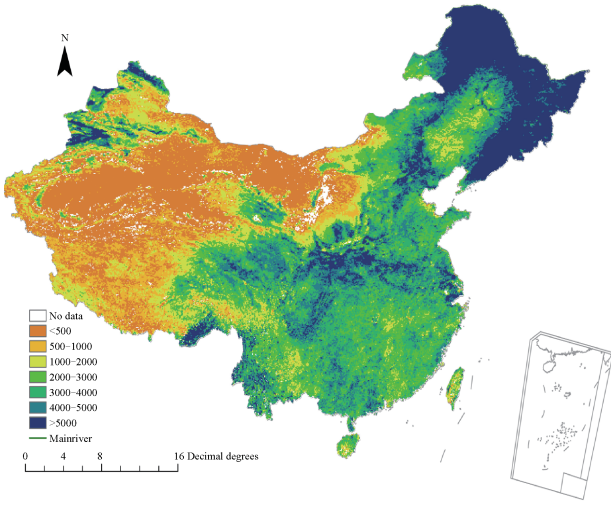

Fig. 2 Small integral over the growing season in 1982 across China

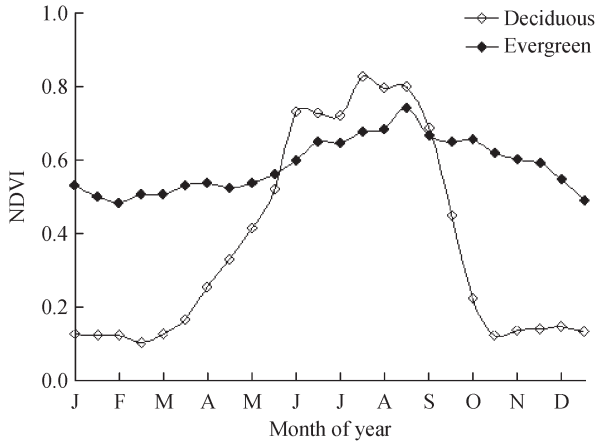

Fig. 3 Different vegetation dynamics explain the difference in small integral in deciduous and evergreen forests. Data was extracted for E'erguna-Zuo Qi in the North-east China (deciduous) and Sanming City in the South-east China (evergreen), respectively, in 1982

The slope of the linear regression between the annual small integral and study year for each pixel with $P \leqslant 0.05$ reveals a significant change in vegetation production across the country from 1982 to 2006. In Fig. 4, positive and negative slope values indicate increasing and decreasing trends, respectively, while white pixels are areas that showed no significant change ($P > 0.05$). The higher the absolute values of the slope, the greater the change in vegetation growth. Results indicate that since 1982, vegetation production had increased in the following regions: 1) Daxing'anling, Xiaoxing'anling areas, Yanshan, Yinshan, and Hetao Plain in Inner Mongolia; 2) Liaoning and Heibei Provinces; 3) Tianshan, Aertaishan, the edges of both Turpan basin and Takelamagan desert in the west; 4) Taihangshan area, and Yulin, Yan'an area in Shanxi Province; 5) some areas in central Jiangxi Province (Fig. 4). Such results are generally consistent with findings from other studies such as those from Myneni et al. (1997), Zhou et al. (2001) and Piao et al. (2004).

Areas that showed a significant decreasing trend were centered in 1) South-east Inner Mongolia and South Heilongjiang; 2) South-west Shannxi; 3) the Yangtze River Delta and some areas along the Yangtze River, such as Minjiang Branch, East Hubei Province, South Anhui and Jiangsu Provinces; 4) Pearl River Delta, and downstream of Mekong River and Brahmaputra River; 5) along the Pacific coast; 6) Jilong, Taibei, Xinzhu, areas from Taizhong to Jiayi, and areas from Hualian to Taidong in Taiwan Province. Areas where decreasing trends were found in this study are much larger than the findings in Piao et al.'s study (2004), in which the maximum monthly 15-day NDVI values were used to represent vegetation change.

To show what could be done with this type of analysis at a local scale and help understand the causes of the change

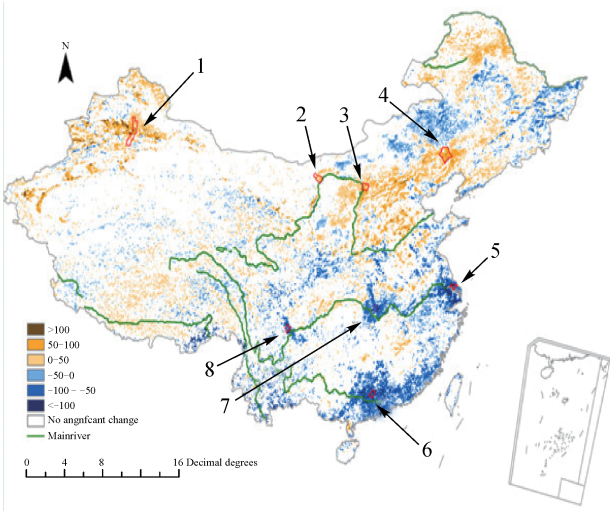

Fig. 4 Trend of vegetation growth during 1982 to 2006, indicated by the slope value of linear relationship between annual small integral over growing season with year ($P \leqslant 0.05$). The number and location names are selected counties that show significant positive or negative trends (see Figs. 5 and 6)

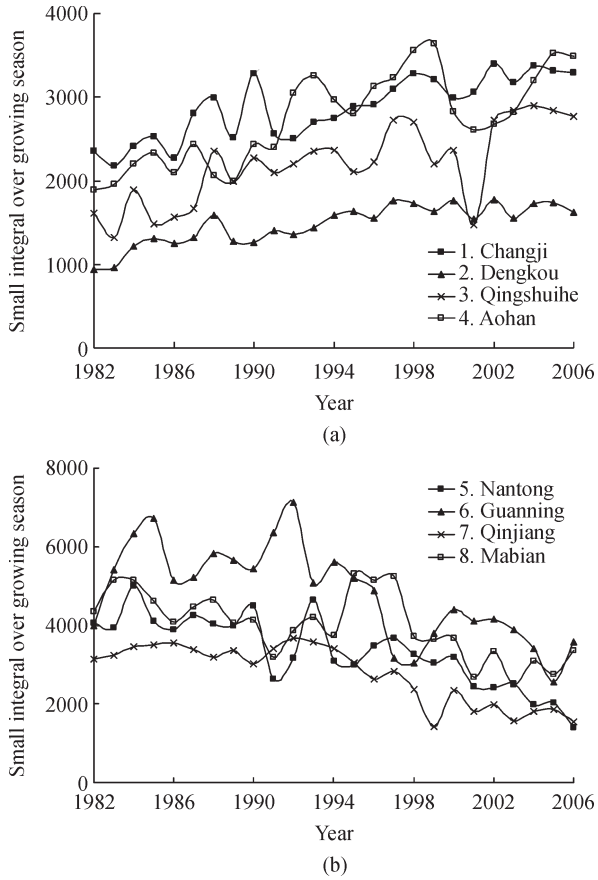

Fig. 5 Examples of positive (upper panel) and negative (lower panel) trends in vegetation growth for eight selected counties

in vegetation production, we selected eight counties from the areas that showed significant changes and examined the trends of the county-averaged small integral values. The locations of the eight counties are shown in Fig. 4. Four of the counties had significant positive trends, and the other four had significant negative trends. Figure 5 shows the time-series of the integral values and Table 1 presents the linear equations and r^2 for each county. The slope of the relationships indicates the degree of the change, and the r^2, ranging from 0.42 to 0.72, indicates the significance of the change.

For each of the eight counties we extracted the annual rainfall to assess the impact of precipitation, since the main drivers of the vegetation change are probably associated with either climate change or human activities. We extracted and averaged the annual precipitation from data downloaded from the China Meteorological Administration for each of the eight counties. We found no significant trends in the annual precipitation for the eight counties through the 25 years of the study period (Fig. 6). The general examination of precipitation shows a lack of significant trend in annual rainfall, which probably indicates that human activities were the primary driver of the vegetation changes in these selected counties. However, this was done only for the selected eight counties and

Table 1 Trend of small integral over growing season at locations indicated in Fig. 4

#	County	Linear regression between the values of annual small integral (y) and time from 1982 to 2006 (x)	r^2
		Positive trends	
1	Changji	$y = 43.18\,x - 83227$	0.72
2	Dengkou	$y = 27.63\,x - 53613$	0.72
3	Qingshuihe	$y = 50.27\,x - 98040$	0.59
4	Aohan	$y = 58.76\,x - 114412$	0.62
		Negative trends	
5	Nantong	$y = -103.87\,x + 210472$	0.70
6	Guanning	$y = -114.19\,x + 232501$	0.48
7	Qianjiang	$y = -87.20\,x + 176636$	0.72
8	Mabian	$y = -73.84\,x + 151233$	0.42

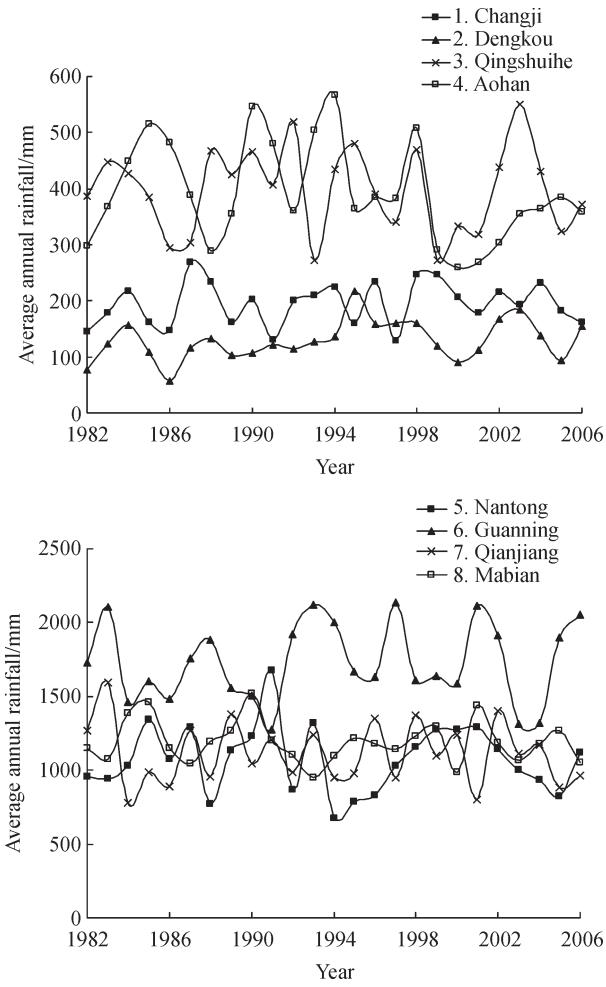

Fig. 6 Time series of annual rainfall during 1982 to 2006 at selected counties indicated there were no significant precipitation changes at these locations

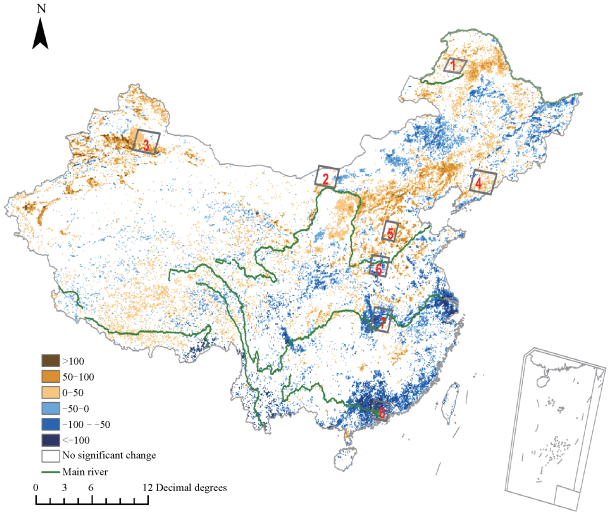

Fig. 7 Location of Landsat image pairs used for validation (quadrangle with number 1–8). Legend refers to Fig. 4

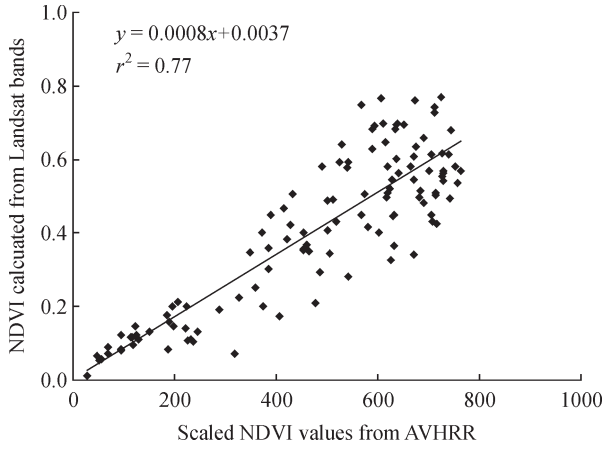

Fig. 8 Validation of AVHRR NDVI using Landsat data

other climate factors such as temperature and soil moisture were not included in this study.

3.2 Validation

Eight pairs of Landsat images were used to validate the NDVI and the trend analysis (Fig. 7). Out of the 16 Landsat images, 11 were taken during 1982–2006 and can be matched with the AVHRR NDVI data used in this study. The Landsat NDVI values were linearly related to the scaled AVHRR NDVI (Fig. 8) values with an r^2 of 0.77, which indicates that AVHRR provided reasonable estimations of the vegetation index given the rather coarse spatial resolution.

Comparison of the vegetation change using classification results from Landsat images confirms the vegetation growth trend obtained in this study using AVHRR data. Table 2 shows the time, sensor, resolution and classified vegetated area for each pair of Landsat images, and the slope of linear trend of the small integral at a county nearby or within the corresponding Landsat image boundary. For example, at the location in Inner Mongolia (#1 image in Fig. 7), the vegetated area increased by 15.4% from Aug 24, 1989 to Jul 13, 2000 (from 10.2% to 11.8%), and the AVHRR trend results gave a slope of 12.9 averaged for a nearby Yakeshi county, which indicates that both Landsat and AVHRR resulted in positive vegetation growth change in this area. In Xinjiang (#2), Liaoning (#4), and Hebei (#5), it increased by 51.7%, 13.6%, and 56.3% from 1970s to 2000s, respectively. In another image from Inner Mongolia (#3), and images from Henan (#6), Hubei (#7) and Guangdong (#8), the vegetation area decreased by 4.6%, 5.5%, 45.3%, and 19.6%, respectively, and these numbers are consistent with the slope of the linear trend generated from AVHRR images.

As examples, the vegetation classification results from Landsat images in Xinjiang (#2 in Fig. 7) and Guangdong (#7) are shown in Fig. 9. Xinjiang is arid and more than

Table 2 Vegetation change at 8 locations based on classification on Landsat images

		Landsat classification results						Trend analysis results from AVHRR for county nearby/within	
#	Location	Date	Satellite	Sensor	Resolution/m	Vegetated area/%	Vegetation change*/%	County name	Slope of the linear trend **
1	Inner Mongolia	24–Aug–1989	Landsat 5	TM	30	10.18	15.40	Yakeshi	12.87
		13–Jul–2000	Landsat 7	ETM +	30	11.75			
2	Xinjiang	13–Aug–1979	Landsat 2	MSS	60	7.78	51.67	Jimusa'er	26.20
		28–Jun–2002	Landsat 7	ETM +	30	11.80			
3	Inner Mongolia	15–Sep–1977	Landsat 2	MSS	60	44.99	−4.58	Wulate-Zhong	−3.48
		14–Sep–2000	Landsat 7	ETM +	30	42.93			
4	Liaoning	5–Jul–1976	Landsat 2	MSS	60	64.37	13.64	Huangren	32.67
		21–Sep–2001	Landsat 7	ETM +	30	73.15			
5	Hebei	3–May–1979	Landsat 2	MSS	60	26.93	56.33	Xingtai	38.23
		7–May–2000	Landsat 7	ETM +	30	42.10			
6	Henan	14–May–1988	Landsat 5	TM	30	47.05	−5.53	Dengfeng	−24.56
		10–May–2000	Landsat 7	ETM +	30	44.45			
7	Hubei	16–Aug–1984	Landsat 2	MSS	60	66.54	−45.34	Xiantao	−74.56
		22–Jul–2001	Landsat 7	ETM +	15	36.37			
8	Guangdong	10–Nov–1979	Landsat 3	MSS	60	81.27	−19.56	Zengcheng	−94.32
		14–Sep–2000	Landsat 7	ETM +	30	65.37			

Notes: * Vegetation change was calculated as: (vegetated area of second image − vegetated area of first image)/vegetated area of first image; ** slope of the linear regression between the values of annual small integral (y) and time from 1982 to 2006 (x), $P \leqslant 0.05$

half of the province is desert or bare rock. The vegetated area in the south had increased significantly as can be seen in Figs. 9(a) and (b). Image #7, located in Guangdong Province, includes part of Hong Kong City. In 1979 (Fig. 9 (c)), the residential area was mostly centralized in the Pearl River Delta and the capital city of Guangzhou. However, in 2001, the residential area extended greatly, especially on the east side of Lingdingyang. The classification results showed that the vegetation area in this region had decreased from 81% to 65% between 1979 and 2001.

There are a number of possible reasons for the discrepancies between the Landsat and AVHRR results. The two sets of NDVI values from AVHRR and Landsat differed not only because of the difference in resolution and satellite sensors, but also because the AVHRR data was taken bi-monthly, and the Landsat NDVI images were calculated from images taken on a single date. Moreover, the trend analysis reflected the vegetation change during 1982 to 2006, while the results from Landsat images revealed the changes between the two specific dates. Finally, the comparisons shown in Table 2 are based on area-averaged results from Landsat images and corresponding county-averaged results from AVHRR NDVI, and often the area of the counties is smaller than the coverage of Landsat image pairs.

4 Discussion

Since the 1970s, China has experienced huge social and economic changes, which had great impacts on land use (Heilig, 1997). As Yabuki (1995) pointed out, the economic reforms of 1978 were probably more important to China's land-use patterns than any other single event in recent history. In 1978, the Chinese government embarked on a policy of opening selected cities to the outside world step by step. In 1979, 4 special economic zones (Shenzhen, Zhuhai, Shantou and Xiamen) along the south-eastern Pacific coast were established; in 1984, 14 other coastal cities from Dalian in Liaoning Province to Beihai in Guangxi Zhuang Autonomous Region were opened; in 1985, the state extended the open economic zones along

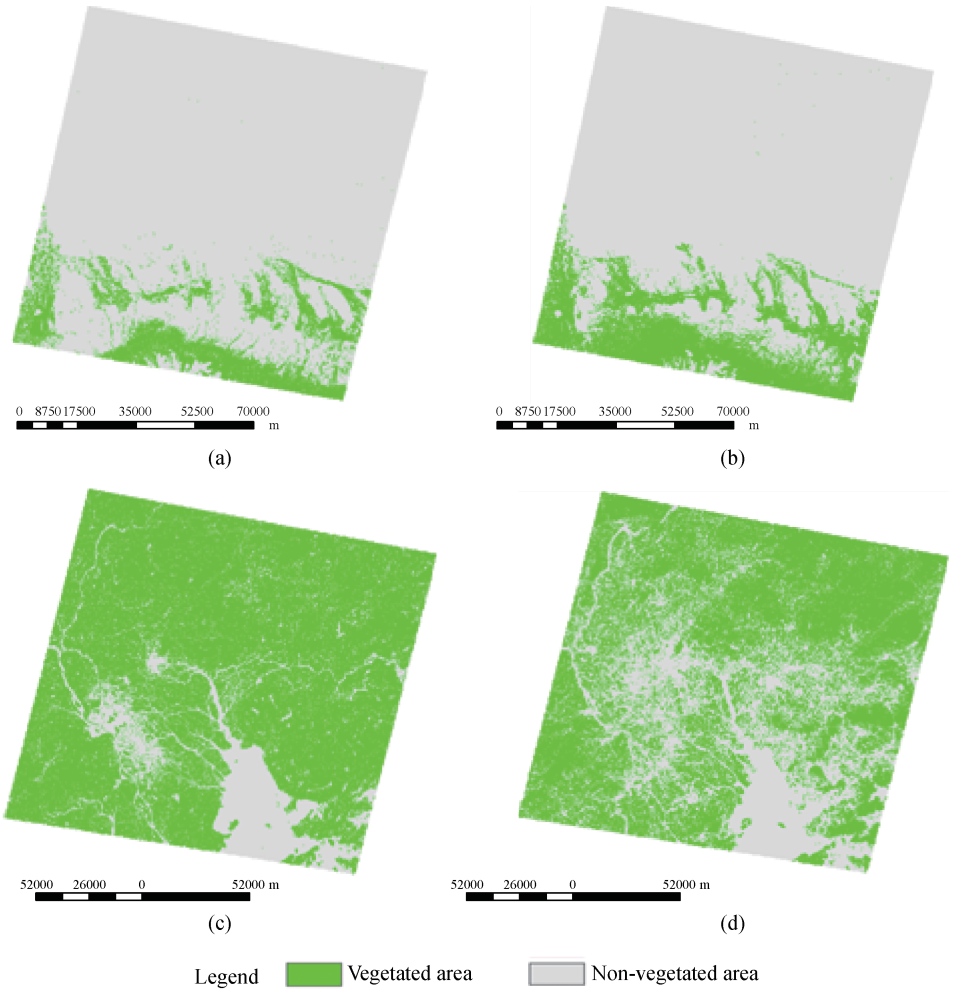

Fig. 9 Vegetation area classified from Landsat image, (a) Xinjiang, Sep 15, 1977; (b) Xinjiang, Sep 14, 2000; (c) Guangdong, Aug 16,1984; (d) Guangdong, July 22, 2001

the coast into an open coastal belt; in 1992, 5 inland cities (Wuhu, Jiujiang, Yueyang, Wuhan, and Chongqing) along the Yangtze River were opened.

The opening of the costal belt and Yangtze River transformed land cover dramatically, and urbanization was one of the results that led to the decrease in vegetation in these areas. For example, data from the Shanghai Municipal Statistics Bureau shows that the cultivated land area in Shanghai decreased by 35% from 1978 to 2005 (Fig. 10). The spatial pattern of significant decreasing trend in Fig. 4 is consistent with findings from Liu et al. (2005) that during 1990 to 2000 there is a remarkable decrease in cropland in the Huang-Huai-Hai Plain, the Yangtze River Delta, the Yellow River band in the vicinity of Baotou and Datong sections, Sichuan Basin, and the Pearl Delta. On the other hand, most of these areas are also located in nationally important food production areas, such as the Songnen Plain and Sanjiang Plain in the north-east, Minjiang watershed located in Chengdu Plain, Jianghan Plain, Jianghuai Plain, and Taihu Plain in the downstream area of the Yangtze River, Boyanghu Plain, and the Pearl Delta, which have had fertile soil and a long history of agricultural activities.

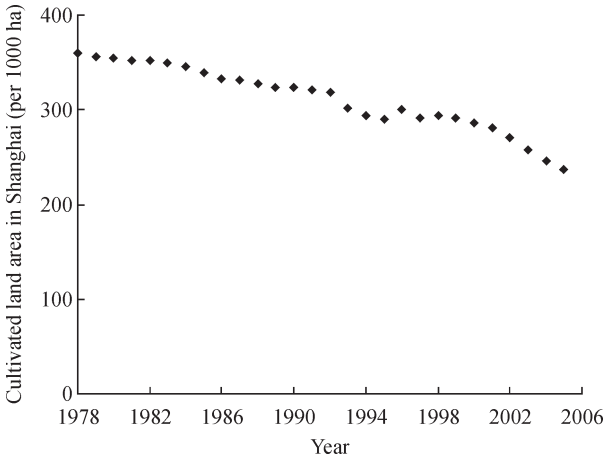

Fig. 10 The cultivated land area in Shanghai decreased 35% from 1978 to 2005, based on data from Shanghai Municipal Statistics Bureau

Along the Yangtze River, besides the rapid urbanization, deforestation in the upper stream of Yangtze River had also taken place and was one of the causes of vegetation reduction. In Inner Mongolia, desertification is another primary cause of vegetation reduction (Yang et al., 2004).

Figure 4 also indicates a significant increase of vegetation production in the north-east, north-west, and central plain, which is consistent with previous studies from Li et al. (2005) and Xu et al. (2004) in North-west China. This shows another example of impact from national policy, the 'Three-North Shelter Forest Programme' launched in 1978. This program is the biggest nation-wide afforestation project in China and covers 4 million km^2 in North China, aiming to restore the forest cover in the mountains, build a crop-shelter forest network in the central plains and oases in the desert, and establish tree belts to protect the grassland, the loess plateau, and desert areas.

In addition, as found by Liu et al. (2005), the cultivated land in Xinjiang, Inner Mongolia, Jilin, Heilongjiang, and Liaoning had increased from 1985 to 1995, which explains the increasing trend in vegetation growth in that area as shown in Fig. 4. Moreover, in North China, regions with access to irrigation also showed a significant increasing trend. For example, in the Hetao Plain where irrigation water is available from the Yellow River, and in areas along the Akesu and Weigan Rivers in Xinjiang, significant positive trends that differ from surrounding areas can be seen in Fig. 4.

5 Conclusions

This study showed that the slope of the linear regression ($P \leqslant 0.05$) between the seasonal small integral computed from long-term AVHRR NDVI can be used to detect vegetation changes across a large spatial region such as China. Validation using Landsat images at a finer resolution confirmed the trend results. This method could be applied to other places and to data from other sensors, such as MODIS, with finer spatial resolution but a shorter study period.

The spatial pattern of the historical trend across China at a pixel level reveals great variation and coincidence with some national policies launched in China since 1978. Significant increasing trends detected in North-east, North-west and Central China indicate the effect of the 'Three-North Shelter Forest Programme' in these areas, while the significant decreases in the grassland area of Inner Mongolia could indicate desertification. Decreasing trends were also found along the coastal area of the Pacific Ocean and some areas along the Yangtze River, which are likely due to the opening of economic zones and inland cities and associated anthropogenic causes such as rapid urbanization and deforestation. Factors causing vegetation production changes are complicated and vary spatially, and more precise data on land use change and management are necessary for more detailed analyses on the exact driving forces of these changes.

References

Chen J, Jönsson P, Tamura M, Gu Z, Matsushita B, Eklundh L (2004). A simple method for reconstructing a high-quality NDVI time-series data set based on the Savitzky–Golay filter. Remote Sens Environ, 91 (3–4): 332–344

Eklundh L, Jönsson P (2003). Extracting information about vegetation seasons in Africa from Pathfinder AVHRR NDVI imagery using

temporal filtering and least-squares fits to asymmetric Gaussian functions. In: Sebastiano B. Serpico, ed. Image and Signal Processing for Remote Sensing VIII. Proceedings of the SPIE (4885): 215–225

Eklundh L, Olsson L (2003). Vegetation index trends for the African Sahel 1982–1999. Geophys Res Lett, 30(8): 1430

European Commission (2003). Global Land Cover 2000 Database. Joint Research Centre

European Space Agency (2004–2006). GlobCover (version 2): Global Land Cover from MERIS

Hansen M, DeFries R, Townshend J, Sohlberg R (1998). UMD Global Land Cover Classification, 1 Kilometer, 1.0, Department of Geography, University of Maryland, College Park, Maryland, 1981–1994

Heilig G K (1997). Anthropogenic factors in land-use change in China. Popul Dev Rev, 23(1): 139–168

Heumann B W, Seaquist J W, Eklundh L, Jönsson P (2007). AVHRR derived phenological change in the Sahel and Soudan, Africa, 1982–2005. Remote Sens Environ, 108(4): 385–392

Jönsson P, Eklundh L (2002). Seasonality extraction by function fitting to time-series of satellite sensor data. IEEE Trans Geosci Rem Sens, 40(8): 1824–1832

Jönsson P, Eklundh L (2003). Seasonality extraction from satellite sensor data. In: Chen C H, ed. Frontiers of Remote Sensing Information Processing. Singapore: World Scientific Publishing. 487–500

Jönsson P, Eklundh L (2004). TIMESAT—a program for analyzing time-series of satellite sensor data. Comput Geosci, 30(8): 833–845

Lee R, Yu F, Price K P, Ellis J, Shi P (2002). Evaluating vegetation phenological patterns in Inner Mongolia using NDVI time-series analysis. Int J Remote Sens, 23(12): 2505–2512

Li H, Wang X, Chen S, Hou P (2005). Dynamic analysis and evaluation of Xinjiang forest resources: based on RS and GIS. J Geogr Sci, 15 (3): 346–352

Liu J, Liu M, Tian H, Zhuang D, Zhang Z, Zhang W, Tang X, Deng X (2005). Spatial and temporal patterns of China's cropland during 1990–2000: an analysis based on Landsat TM data. Remote Sens Environ, 98(4): 442–456

Lloyd D (1990). A phenological classification of terrestrial vegetation cover using shortwave vegetation index imagery. Int J Remote Sens, 11(12): 2269–2279

Lucht W, Prentice I C, Myneni R B, Sitch S, Friedlingstein P, Cramer W, Bousquet P, Buermann W, Smith B (2002). Climatic control of the high-latitude vegetation greening trend and Pinatubo effect. Science, 296(5573): 1687–1689

Markon C J, Fleming M D, Binnian E F (1995). Characteristics of vegetation phenology over the Alaskan landscape using AVHRR time-series data. Polar Rec (Gr Brit), 31(177): 179–190

Mather P M (2004). Computer Processing of Remotely Sensed Images: an Introduction. Chichester: John Wiley & Sons

Moulin S, Kergoat L, Viovy N, Dedieu G (1997). Global-scale assessment of vegetation phenology using NOAA/AVHRR satellite measurements. J Clim, 10(6): 1154–1170

Myneni R B, Keeling C D, Tucker C J, Asrar G, Nemani R R (1997). Increased plant growth in the northern high latitudes from 1981–1991. Nature, 386(6626): 698–702

Piao S, Fang J, Ji W, Guo Q, Ke J, Tao S (2004). Variations in a satellite-based vegetation index in relation to climate in China. J Veg Sci, 15 (2): 219–226

Piao S, Fang J, Zhou L, Ciais P. Zhu B (2006). Variations in satellite-derived phenology in China's temperate vegetation. Global Change Biology, D12103(12): 14

Raynolds M K, Walker D A, Maier H A (2006). NDVI patterns and phytomass distribution in the circumpolar Arctic. Remote Sens Environ, 102(3–4): 271–281

Slayback D A, Pinzon J E, Los S O, Tucker C J (2003). Northern hemisphere photosynthetic trends 1982–99. Glob Change Biol, 9(1): 1–15

Tucker C J, Pinzon J E, Brown M E, Salyback D A, Pak E W, Mahoney R, Vermote E F, Saleous E N (2005). An extended AVHRR 8-km NDVI data set compatible with MODIS and SPOT vegetation NDVI data. Int J Remote Sens, 26(20): 4485–4498

Tucker C J, Slayback D A, Pinzon J E, Los S O, Myneni R B, Taylor M G (2001). Higher northern latitude NDVI and growing season trends from 1982 to 1999. Int J Biometeorol, 45: 184–190

White M A, Hoffman F, Hargrove W W, Nemani R R (2005). A global framework for monitoring phenological responses to climate change. Geophys Res Lett, 32(4): L04705

White M A, Thornton P E, Running S (1997). A continental phenology model for monitoring vegetation responses to interannual climatic variability. Global Biogeochem Cycles, 11(2): 217–234

Xu W, Wu B, Yan C (2004). Detecting vegetation change during the period 1998–2002 in NW China using SPOT-VGT NDVI time-teries data. IEEE International Geoscience and Remote Sensing Symposium, 3417–3419

Yabuki S (1995). China's New Political Economy: the Giant Awakes. Boulder: Westview Press

Yang S, Shi Z, Zhao H, Li P, Dai S, Gao A (2004). Effects of human activities on the Yangtze River suspended sediment flux into the estuary in the last century. Hydrol Earth Syst Sci, 8(6): 1210–1216

Zhang X, Friedl M A, Schaaf C B (2006). Global vegetation phenology from moderate resolution imaging spectroradiometer (MODIS): evaluation of global patterns and comparison with in situ measurements. Journal of Geophysical Research, G04017(111): 14

Zhang X, Friedl M A, Schaaf C B, Strahler A H, Hodges J C, Gao F, Reed B, Huete A (2003). Monitoring vegetation phenology using MODIS. Remote Sens Environ, 84(3): 471–475

Zhou L M, Tucker C J, Kaufmann R K, Slayback D, Shabanov N V, Myneni R B (2001). Variations in northern vegetation activity inferred from satellite data of vegetation index during 1981 to 1999. J Geophys Res Atmos, 106(D17): 20069–20083

Haiyan Wei is an assistant research scientist at the University of Arizona. She earned her Ph.D. in Watershed Management, with a minor in Remote Sensing. Her area of interest includes hydrology and erosion modeling, remote sensing application, and rangeland drought management.

Philip Heilman is the Research Leader at the Southwest Watershed Research Center. He has an undergraduate degree in Economics and Ph.D. in Watershed Management, with minors in Agricultural Economics and Management Information Systems. His research interests include decision support systems, water quality, rangeland management, and natural resource economics.

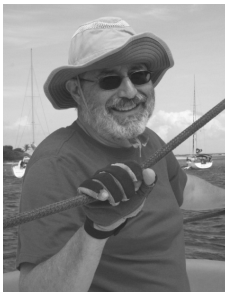

Mark A. Nearing is a research scientist at the Southwest Watershed Research Center in Tucson, Arizona. His area of research includes 1) determining sustainable land use and management practices with regard to soil, water, plant, and other watershed resources, 2) developing suitable computer simulation models to assess soil sustainability, 3) incorporating new technologies into the models and new measurement technologies into field experiments, and 4) developing technology transfer to disseminate research findings and results to land managers and decision makers. Dr. Nearing has authored more than 300 scientific papers, including more than 120 refereed scientific journal articles. Most of his research has been in the area of soil erosion research, including understanding basic erosion processes, field measurement techniques, computer simulation modeling, and understand global change impacts on erosion and conservation. He is past President and serves on the Board of Directors of the International Soil Conservation Organization, was a contributing author to Working Group II, Ch. 3, regarding the impacts of climate change on soil erosion to the 4th IPPC (Intergovernmental Panel on Climate Change) Assessment report, 2007, and is a Fellow of the Soil Science Society of America.

Zhihui Gu obtained her Ph. D. in Environmental Change and Regional Planning from Beijing Normal University, China. She is currently an assistant research professor at the college of Architecture and Urban Planning, Shenzhen University, China. Her area of expertise includes biological applications of remote sensing and urban disaster risk assessment.

Yongguang Zhang obtained his Ph.D. degree of physical geography from Beijing Normal University, China. He is currently an assistant research scientist at USDA-ARS Southwest Watershed Research Center and the University of Arizona. His area of research includes soil erosion, the impacts of climate change on soil and water conservation, and the climate extremes effects on terrestrial ecosystem productivity.